Development/Plasticity/Repair

Mature Mice Lacking *Rbl2*/p130 Gene Have Supernumerary Inner Ear Hair Cells and Supporting Cells

Sonia M. Rocha-Sanchez,[1] Laura R. Scheetz,[1] Melissa Contreras,[1] Michael D. Weston,[1] Megan Korte,[2] JoAnn McGee,[2] and Edward J. Walsh[2]

[1]Department of Oral Biology, Creighton University School of Dentistry, Omaha, Nebraska 68178, and [2]Developmental Auditory Physiology Laboratory, Boys Town National Research Hospital, Omaha, Nebraska 68131

Adult mammalian auditory hair cells (HCs) and their associated supporting cells (SCs) do not proliferate, and HC death leads to irreversible neurosensory hearing loss and balance impairment. In nonmammalian vertebrates, loss of HCs induces mitotic proliferation of adjacent nonsensory SCs and/or direct SC transdifferentiation to generate replacement cells. This results in the structural and functional recovery of the nonmammalian sensory systems. Potential replacement of mammalian auditory HCs, either by transplanting cells or by transforming existing cells through molecular therapy, has long been proposed. However, HC replacement strategies with clear therapeutic potential remain elusive. The retinoblastoma (pRB) family of cell cycle regulators, *Rb1*, *Rbl1* (p107), and *Rbl2* (p130), regulate the G_1- to S-phase transition in proliferating cells. In the inner ear, the biochemical and molecular pathways involving pRBs, particularly p107 and p130, are relatively unexplored and their therapeutic suitability is yet to be determined. In this study, we analyzed the cochleae of adult p130 knock-out ($p130^{-/-}$) mice and showed that lack of the p130 gene results in extra rows of HCs and SCs in the more apical regions of the cochlea. No evidence of transdifferentiation of these supernumerary SCs into HCs was observed in the $p130^{-/-}$ mouse. Nevertheless, unscheduled proliferation of SCs in the adult $p130^{-/-}$ cochlea coupled to downregulation of bona fide cell cycle inhibitors provides a mechanistic basis for the role of p130 as a regulator of SC and HC mitotic quiescence in the more apical regions of the cochlea. Interestingly, $p130^{-/-}$ mice exhibited nearly normal peripheral auditory sensitivity.

Introduction

Like other neuron-derived cells, commitment of inner ear sensory precursors to a particular fate is controlled by a series of highly organized events involving sequential signals that regulate cell cycle exit, cell survival, quiescence, and terminal differentiation. Terminally differentiated mammalian auditory sensory hair cells (HCs) and associated supporting cells (SCs) remain mitotically quiescent throughout life and cannot regenerate after trauma, leaving mammals vulnerable to permanent hearing impairment. In nonmammalian vertebrates, in which cellular and functional regeneration have been documented, SCs are the major source of new HCs (Jones and Corwin, 1993; Cotanche, 1997; Taylor and Forge, 2005; Hernández et al., 2007; Stone and Cotanche, 2007). Likewise, mammalian SCs can be forced to transdifferentiate into HCs (Kawamoto et al., 2003; Shou et al., 2003; Woods et al., 2004; Yamasoba and Kondo, 2006). However, the overall therapeutic effectiveness of direct SC-to-HC transdifferentiation in mammals is seriously limited by the consequent loss of SCs that play equally important roles for normal mechanoelectrical transduction. Therefore, regeneration of HCs at the expense of existing SCs does not solve the problem; indeed, it creates a new one.

Establishing therapeutic measures that slow the progression of hearing loss or restore lost hearing is a major clinical challenge. However, HC replacement strategies with clear therapeutic application remain elusive. A potential regeneration strategy being considered in mammals is the induction of new HCs through manipulation of the cell cycle machinery of existing HCs or SCs (Rocha-Sanchez and Beisel, 2007). Currently, neither the mechanism leading to the permanent mitotic quiescence of HCs and SCs, nor the process through which auditory cells are able to reenter the cell cycle and proliferate in either nonmammalian or mammalian vertebrates is understood (Morest and Cotanche, 2004; Duncan et al., 2006; Cafaro et al., 2007; Rocha-Sanchez and Beisel, 2007). The retinoblastoma (pRB) family, namely *Rb1*, *Rbl1* (p107), and *Rbl2* (p130), plays a critical role in the cell cycle by actively interacting with and repressing the transcription of genes that are important in proliferation and differentiation (Cobrinik, 2005; Rocha-Sanchez and Beisel, 2007). In the inner ear, *Rb1* is known to affect proliferation, maturation, and survival of HCs. Partial or complete elimination of *Rb1* results in massive proliferation of HCs and to some extent SCs, followed by apoptotic death of all sensory cells in the cochlea (Mantela et al., 2005; Sage et al., 2005, 2006; Weber et al., 2008; Yu et al., 2010).

Received Nov. 5, 2010; revised April 14, 2011; accepted April 20, 2011.

Author contributions: S.M.R.-S. designed research; S.M.R.-S., L.R.S., M.C., M.D.W., M.K., J.M., and E.J.W. performed research; S.M.R.-S., M.D.W., J.M., and E.J.W. analyzed data; S.M.R.-S., J.M., and E.J.W. wrote the paper.

This work was supported in part by NIH–NIDCD Grant 5R03DC9989, NIH–Centers of Biomedical Research Excellence–NCRR Grant P20 RR018788-06A (S.M.R.-S.), and NIH–NCRR Grant G20RR024001 (Creighton University Animal Research Facility). We thank Dr. Venkatesh Govindarajan for critical reading and helpful discussion and University of Nebraska Medical Center Molecular Phenotyping Core and Anita Jennings for valuable technical assistance. The confocal microscopic system was made available by the Nebraska Center for Cell Biology at Creighton University.

Correspondence should be addressed to Sonia M. Rocha-Sanchez, Department of Oral Biology, Creighton University School of Dentistry, Boyne Building, Room 313, Omaha, NE 68178. E-mail: ssanchez@creighton.edu.

DOI:10.1523/JNEUROSCI.5821-10.2011

 0270-6474/11/318883-11$15.00/0

What role the other pRB family members play in the inner ear is unknown. To investigate the function of p130 in the cochlea and its potential as an agent of HC and SC proliferation, we have examined the cochlea and assessed the functional integrity of the auditory periphery of adult mice with a targeted mutation in the p130 gene. In the absence of p130, extra rows of SCs, inner hair cells (IHCs), and outer hair cells (OHCs) are present in the apex and upper middle turns of the cochlea. Interestingly, p130$^{-/-}$ mice exhibit nearly normal peripheral auditory sensitivity.

Materials and Methods

Animals

In contrast to *Rb1* deficiency, germ line p130-deficient mice are viable and exhibit minimal developmental abnormalities (Cobrinik et al., 1996). Targeted p130 knock-out (p130$^{-/-}$) mice were obtained from Dr. Tyler Jacks (Massachusetts Institute of Technology, Cambridge, MA) and crossed to C57BL/6 mice purchased from Charles River Laboratories. The mutation was generated by joining the mouse p130 gene at codon 102 to the neo cassette, causing an in-frame substitution of three amino acids followed by an in-frame termination at codon 106 (Cobrinik et al., 1996). Embryonic, neonatal, and adult male and female experimental animals were genotyped by PCR following procedures described previously (Cobrinik et al., 1996) or by Transnetyx. Wild-type (WT) and p130$^{-/-}$ PCR products were purified and sequenced using an ABI Prism 3100 genetic analyzer to confirm the mutation site. All tissues were harvested from male and female animals in accordance with the Creighton University Institutional Animal Care and Use Committee-approved protocol number 0853.

In vivo *functional assessment*

Auditory brainstem responses (ABRs) and distortion product otoacoustic emissions (DPOAEs) were recorded from male and female WT and p130$^{-/-}$ animals on approximately postnatal day 30 (P30). Mice were anesthetized with a ketamine–xylazine mixture (100 mg/kg ketamine, 15 mg/kg xylazine, i.p.) and supplemented with 25–50% of the initial dose as needed throughout the recording session to maintain a stable and quiet recording environment. Body temperature was controlled using a thermostatically regulated heating blanket and thermal probe, and body temperature was maintained at ~37.5°C (Harvard Apparatus). Heart rate was monitored throughout the procedure and fluids were replaced as needed. All recordings were conducted in an electrically shielded, double-walled sound-attenuating chamber (Industrial Acoustics). This study was approved by the Boys Town National Research Hospital Institutional Animal Care and Use Committee.

ABR procedures

ABRs were used to assess the integrity of the cochlea and auditory brainstem noninvasively (Walsh et al., 1986). Platinum subdermal needle electrodes (Grass Instruments) were positioned at the vertex (active, noninverting), infra-auricular region (reference, inverting), and in the neck region (ground). Differentially recorded scalp potentials were amplified 100,000× and bandpass filtered between 0.03 and 10 kHz (Grass Instruments model P511K), and digitized (Tucker-Davis Technologies) using a 20 kHz sampling rate over a 15 ms epoch. A total of 200 trials was averaged for each waveform and each stimulus condition was replicated. Trials with extraneously high voltages because of muscle or ECG artifact were excluded from the average, and the trial was repeated. On completion of a run, response waveforms were stored digitally for off-line analyses. Custom software was used for data acquisition and subsequent analyses.

Stimuli consisted of symmetrically shaped tone bursts that were 3 ms long (1 ms raised cosine on/off ramps and 1 ms plateau) and clicks that were 64 μs in duration. Both clicks and tone bursts were generated digitally using a clock rate of 125 kHz and delivered free-field via a high impedance piezoelectric tweeter (Radio Shack), and an electrostatic speaker (ES1; Tucker-Davis Technologies) was used to deliver tone bursts >32 kHz. The sound source was placed 10 cm from the animal's vertex, and stimulus levels were calibrated using a 1/8 inch Brüel & Kjær microphone (model 4138) positioned at the approximate location of the subject's head during recording sessions and are reported in decibels sound pressure level (dB SPL: referenced to 20 μPa). Stimuli of alternating polarity were delivered at an interval of 80 ms. ABR thresholds were determined for clicks and for tone bursts in half-octave steps ranging from 64 to 2.0 kHz. Stimulus levels ranged from 90 dB SPL to below threshold in 10 dB steps. Near threshold, levels were changed in 5 dB steps. Threshold was defined as the lowest stimulus level eliciting an unambiguous, replicable response.

DPOAE procedures

DPOAEs were used to assess OHC function noninvasively (Walsh and McGee, 2001). Stimuli consisted of two phase-locked tones of different frequency ($f_1 < f_2$) generated by 24 bit D/A converters (Lynx22 soundcard) and delivered to separate earphones, so that the output of the two tones combined acoustically. Electrostatic speakers (Tucker-Davis Technologies EC1 phones) were used generally; however, for stimuli <5 kHz, ER2 earphones (Etymotic Research) were used. Primary frequencies were adjusted to an f_2/f_1 ratio of ~1.25 and the level of f_2 was set 10 dB lower than f_1. The earphone outputs, along with a low-distortion probe microphone (Etymotic Research; ER-10B+) were sealed within the external ear canal, forming a closed acoustic system. The microphone signal was amplified 40 dB and synchronously sampled with a 24 bit A/D converter (Lynx Studio Technology; L22) at a 192 kHz sampling rate at frequencies >5 kHz, and at a rate of 48 kHz, <5 kHz. Artifact rejection was used to eliminate signals containing extraneous noise. The digitized signals were separated into two independent buffers and averaged over repeated trials until one of three criteria was met: the period of averaging equaled 30 s, the noise floor equaled or fell below −30 dB SPL, or the signal-to-noise ratio equaled or exceeded 30 dB. The sum of the two partial averages was used to obtain the DPOAE (as well as stimulus levels recorded in the ear canal), and the difference was used to estimate the noise floor. Stimulus levels were calibrated *in vivo* at the beginning of every measurement series (approximately every 5–10 min) using the probe microphone. FFT analyses were used on-line and off-line to compute levels and phases of component DPOAEs and corresponding noise floors. Temporal waveforms were stored digitally for subsequent off-line analyses.

Results from the p130$^{-/-}$ mice were compared with WT mice using a two-way mixed ANOVA, with genotype as the between-subjects variable and stimulus frequency as a repeated measure. Differences were considered statistically significant when $p < 0.05$. After functional analyses, animals were killed and their temporal bones were dissected for anatomical and/or expression analyses.

Semithin sections

Inner ear tissues of P30 male and female WT and p130$^{-/-}$ animals were gently perfused with 4% PFA in PBS through the round window, immersed in the same fixative for 24 h at 4°C, and decalcified in 0.1 M EDTA/PBS, pH 7.4. After decalcification, the cochlear neurosensory epithelia, the organ of Corti (OC), was dissected in PBS, embedded in epoxy resin using the Embed 812 kit (Electron Microscopy Sciences) following the manufacturer's instructions, and cut into 3-μm-thick sections. Sections were stained with 0.1% toluidine blue (w/v in water) for 20 s and analyzed using a Nikon Eclipse 80i microscope.

Immunohistochemistry

Immunolocalization of p130 (Abcam), acetylated α-tubulin (Zymed), β-tubulin (Sigma-Aldrich), SOX2 (Millipore), myosin VIIa (Proteus Biosciences), p75^{NTR} (Millipore Bioscience Research Reagents), and CDKN1B (Abcam) proteins was performed on formalin-fixed whole-mount preparations or paraffin-embedded 4-μm-thick cross sections of dissected male and female WT and p130$^{-/-}$ cochlear neurosensory epithelia—the OC. Tissue pieces or sections of the OC (apex, middle, and base) were block/permeabilized with 5% NGS/0.1% Tween 20 at room temperature for 2–3 h, incubated with a primary antibody for 48 h (whole mount) or 3 h (cross sections) in blocking buffer, and washed three times with PBS. Samples were then labeled with either Alexa 488- or Alexa 568-conjugated secondary antibodies (1:500) (Invitrogen), washed with PBS, coverslipped using Prolong anti-fade (Invitrogen), and

analyzed using a Zeiss LMS 510 confocal microscope. All samples were processed using antigen retrieval. Fixed and dissected tissue pieces were transferred to 0.1 M citrate buffer, pH 7.0, and heated to 125°C for 30 s followed by 90°C for 10 s before the standard immunohistochemistry procedures.

Quantification of p130 expression gradient

Whole-mount P30 mouse OC stained with both 4′6-diamidino-2-phenylindole (DAPI) and p130 antibody were flat-mounted using antifade medium, and *Z*-stacks of the entire depth of the OC were imaged using a Zeiss LMS 510 confocal microscope at 400× magnification. The same parameters were used to collect color (RGB) images from apex, middle, and basal regions of the OC. A subset (16 μm depth) of the entire *Z*-stack series centered on IHC nuclei were collapsed using the LMS image browser software, and these single images were opened in MetaMorph 7.5.6.0 (Molecular Devices). A drawing tool was used to create and center circles of the same diameter on 10 apical, 10 middle, and 10 basal IHC nuclei. The raw average pixel intensity within each circle was collected from the red (p130) and blue (DAPI) channels. Raw average pixel intensities of each nucleus were normalized by subtracting the average pixel intensity of the entire image for each channel. The ratio of p130 to DAPI fluorescence for all 30 nuclei was calculated using both the raw and normalized pixel intensities. The resulting ratio values were rank transformed and grouped into apex, middle, and base IHC nuclei. The Kruskal–Wallis one-way ANOVA on rank was applied to determine whether ratio values among the three locations were statistically distinct. Significant differences between each group were performed using Mann–Whitney pairwise tests. Statistical tests using p130/DAPI ratio calculated from either raw or normalized pixel intensities yielded similar *p* values. The p130/DAPI ratios using normalized pixel intensities are reported for simplicity.

Proliferation assay

To label mitotically active cells, a single, subcutaneous injection of the thymidine analog 5-ethynyl-2′-deoxyuridine (EdU) (50 mg/kg) in DMSO was administered to P21 and P30 male and female WT and $p130^{-/-}$ mice 4 h before tissue harvesting. EdU incorporation into DNA of whole-mount OC was detected using the Click-iT EdU Alexa 488 Fluor Imaging kit (Invitrogen) and double stained with DAPI following the manufacturer's instruction and experimental procedures described previously (Kaiser et al., 2009). Samples were imaged using a Zeiss LMS 510 confocal microscope.

Immunoprecipitation followed by Western blot

Cochlear extract preparation. Cochleae of P30 male and female WT and $p130^{-/-}$ mice were dissected away from their attached vestibular regions and immediately frozen in liquid nitrogen. Frozen cochleae were pooled and homogenized in 300 ml of ice-cold homogenizing lysis buffer (100 mM Tris-HCl, pH 7.4, 150 mM NaCl, 0.5 mM $MgCl_2$, 0.5 mM $CaCl_2$, 1% Brij97) containing Complete Mini EDTA-Free for protease inhibition (Roche Applied Sciences). Cochlear extracts were cleared by centrifugation at 3000 rpm for 8 min at 4°C, and the supernatant was stored at −80°C until use. The protein content of the samples was determined with the Agilent Protein 230 kit (Agilent Technologies).

Immunoprecipitation. For immunoprecipitation, 30 μl of protein G beads (Sigma-Aldrich) were combined with 5 μl of purified mouse IgG serum (Invitrogen) or monoclonal p130 antibody (Abcam), for control and experimental samples, respectively, and incubated overnight at 4°C to allow for prebinding. Next, 500 μg of cochlear protein lysate was added to 300 μl of prebound beads, spun down for 5 s at 3000 rpm, and incubated overnight at 4°C. To prepare samples for electrophoresis, the mix of protein lysate/G beads was spun down at 3000 rpm for 5 s at 4°C; supernatant was discarded, and 500 μl of lysis buffer was added to the beads, before spinning the mixture down under the same conditions as described above. Once the supernatant was discarded, beads were resuspended in 40 μl of 5× Lammeli buffer (0.5 M Tris-HCl, 13% glycerol, 10% SDS, 6% 2-β-mercaptoethanol) and stored at −20°C until use.

Western blot analysis. Equal amounts of cochlear protein were subjected to SDS-PAGE on Criterion precast 10% polyacrylamide gels, and the proteins were then transferred to PVDF membranes in a Bio-Rad TransBlot apparatus according to the manufacturer's instructions. After incubation with a blocking solution, the membranes were probed overnight at 4°C with monoclonal primary antibody against p130 (Abcam). All antibodies were diluted 1:1000 in blocking solution. The membranes were then washed and incubated with the appropriate HRP-conjugated secondary antibodies overnight at 4°C. Immunoreactive bands were visualized on a Kodak Gel Logic 2200 digital imaging system (Carestream Health).

Real-time quantitative PCR

Total RNA from whole otocyst/early-stage cochlea of WT mice between embryonic day 12.5 (E12.5) to E14.5 and from dissected OC of P0, P14, and P35 male mice was obtained as described previously (Rocha-Sanchez et al., 2007) and purified using the RNeasy kit (QIAGEN). Up to 20 μg of total RNA were treated with RNase-free DNase (Turbo DNfree; Ambion), and RNA purity and quality were assessed on a Nanodrop spectrophotometer and Agilent Bioanalyzer, respectively. Using random hexamers for reverse transcription (RT) with MMLV (Invitrogen; ABI), 1–5 μg of total RNA was converted to cDNA. TaqMan PCR assays (Applied Biosystems; StepOne plus system) for the three pocket proteins (i.e., *Rb1*, p107, p130), and the cyclin-dependent kinase inhibitor (CKI) *Cdkn1b* ($p27^{Kip1}$) were performed in quadruplicate for each genotype and relative quantitation of mRNA abundance was normalized to endogenous β-Actin using StepOne Software (Applied Biosystems; version 2.1). *T* tests were performed on the normalized gene expression values to determine whether differences were statistically significant. A value of $p \leq 0.01$ was considered significant.

Cell counting

Counting of supernumerary rows of OHCs, IHCs, and Deiters' cells, as well as individual supernumerary pillar cells was performed on reconstructed confocal stacks using NIH ImageJ 1.4 software. *t* tests were used to statistically compare the number of supernumerary HCs and SCs in the apex and middle turns of $p130^{-/-}$ and WT cochleae. A value of $p \leq 0.01$ was considered significant.

Results

p130 expression in the wild-type cochlea

To determine the spatial expression of p130 in various cells in the OC, commercially available monoclonal anti-p130 antibody was used to immunolabel mouse p130 protein. At P0, p130 immunoreactivity was detected in the SCs throughout the length of the cochlea (Fig. 1*A*,*B*), but not in the HCs (data not shown). Consistent with p130 protein undergoing postnatal developmental expression changes, an apex-to-base gradient was observed at P14 and P30 with p130 protein being observed in the nuclei of both types of HCs, as well as in their associated SCs (Fig. 1*C–J*). Moreover, p130 immunoreactivity did not exceed background level in the basal turn OC at either P14 or P30 (data not shown). To quantify the longitudinal gradient of p130 nuclear labeling, we used MetaMorph software to determine the average pixel intensity of 30 IHC nuclei immunofluorescently stained for p130 protein and colabeled with the nuclear dye DAPI, as described in Material and Methods. The mean ratio of p130/DAPI-stained IHC nuclei was 1.90 ± 0.33 (apex), 0.43 ± 0.11 (middle), and 0.23 ± 0.25 (base). A significant difference in the ratio value among the three groups of IHC nuclei was found (Kruskal–Wallis ANOVA, $H = 20.78$, $p < 0.0001$). The p130/DAPI IHC nuclei ratio was significantly higher in apical IHCs compared with either middle or basal IHC (Mann–Whitney pairwise test, $p < 0.001$). No significant difference was found between middle and basal IHC with respect to p130 immunolabel normalized to DAPI-stained nuclei (Mann–Whitney pairwise test, $p = 0.07$). These data support the notion of a p130 expression gradient in sensory cells in the OC. The existence of a longitudinal apex-to-base gradient for p130 in the mouse OC from P14 onward resembles that

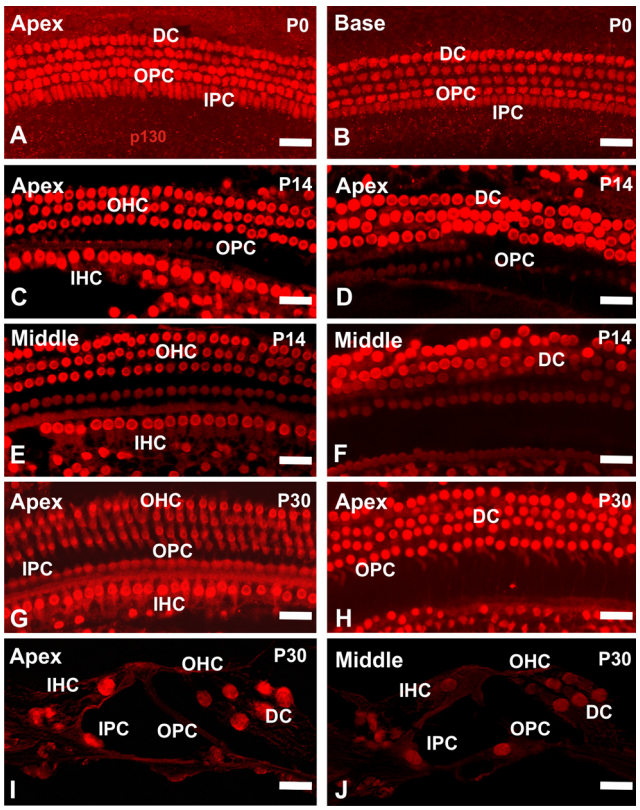

Figure 1. Spatiotemporal expression of p130 in the WT mouse OC. ***A***, ***B***, At birth (P0), p130 protein expression was equally detected throughout the length of the OC. No HC expression was observed in the neonatal OC. ***C–F***, Developmental regulation of p130 expression was noticeable by P14. At this time point, p130 immunolabeling was detectable in both apical and middle turn HCs (***C***, ***E***) and SCs (***D***, ***F***). p130 protein expression in the basal turn was at background level (data not shown). ***G–J***, Similar to P14, p130 protein was detected in HCs and SCs following an apex-to-base gradient, with no detectable expression in the basal turn (data not shown). Cross-sectional immunolabeling (***I***, ***J***) reveals details of p130 protein expression in the apical and middle turns of the OC at P30. OHC, Outer hair cells; IHC, inner hair cells; IPC, inner pillar cells; OPC, outer pillar cells; DC, Deiters' cells. Scale bar, 10 μm.

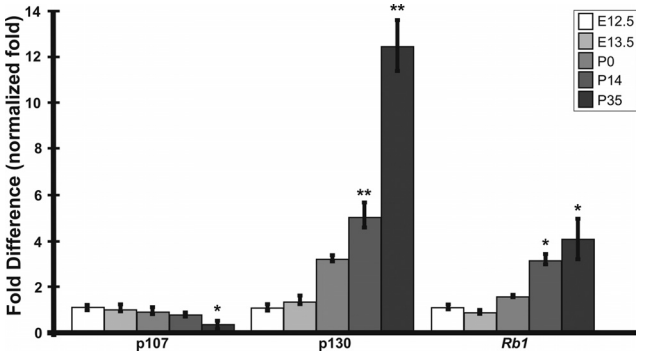

Figure 2. Temporal expression of p130 compared with the other pRBs in the inner ear sensory epithelia. Real-time quantitative PCR analysis of p107, p130, and *Rb1* was performed in subdissected otocyst (E12.5 and E13.5) and organs of Corti (P0–P35) from WT mice at five different stages of inner ear development. Data set of four otocysts or four subdissected OC per time point were analyzed four times, normalized to actin, and averaged. The SDs were within 1% of the mean. Consistent with the idea of p130 playing a role in maintaining mitotic quiescence in the adult OC, p130 as well as *Rb1* levels increase significantly in the postmitotic OC. Conversely, p107 levels decrease, particularly in postmitotic OC. $*p < 0.01$; $**p < 0.001$.

described previously for CDKN1B ($p27^{Kip1}$) expression in the OC (Chen and Segil, 1999). However, although CDKN1B appears to follow a radial gradient of expression in the adult OC (i.e., higher in Hensen's cells) (Minoda et al., 2007), p130 seems to be equally expressed across the radial extent of the OC (Fig. 1*A–J*).

Temporal expression of p130 mRNA in the OC was evaluated by RT-PCR analyses during the developmental period that sensory HCs and SCs develop and reach maturity (i.e., E12.5, E13.5, P0, P14, and P35) (Fig. 2). The specific time points selected for analysis were based on estimates of relative mitotic activity during the overall period of OC maturation, as well as the functional status of the cochlea during postnatal maturation. For example, at E12.5, both sensory and nonsensory precursor cells are actively mitotic, whereas by E14.5 they have become postmitotic; mitotic activity in the OC has ceased by P0 (Ruben, 1967). The first responses to intense airborne sounds have been observed in mice at approximately P10 or P11, and by P30 the OC is completely adultlike from a physiological perspective. Relative abundance of p130 transcript is consistently low around the mitotic phase of HC and SC progenitor cells in the embryonic OC. Conversely, p130 relative expression increases significantly from birth (P0) onwards, reaching its highest relative levels at P35 (Fig. 2).

Previous reports of *Rb1* expression in the inner ear suggest that *Rb1* is expressed during the mitotic and postmitotic periods in the OC (Mantela et al., 2005; Sage et al., 2005). As such, *Rb1* was used as an internal control, and relative expression at E12.5 was compared with the other pRBs in WT mice. Results confirmed and extended previous findings for *Rb1* and provide evidence that *Rb1* and p130 transcripts, but not p107, appear developmentally upregulated in the OC. As a whole, p107 mRNA levels are consistently low at all time points studied, but significantly lower in the mature OC ($p < 0.01$). Similar to p130, *Rb1* transcript levels become increasingly elevated from the time OC cells are exiting the cell cycle (i.e., around E13.5) and reach significantly higher levels by P35. Notably, relative p130 mRNA abundance in the postmitotic OC is considerably higher than that for *Rb1* ($p < 0.01$) (Fig. 2), suggesting a non-overlapping role for p130 and *Rb1* in the quiescent OC of the adult mouse inner ear.

Mature OC phenotype in the absence of a functional p130 gene

In an effort to identify differences between the OC phenotype of WT and $p130^{-/-}$ mice, 23 $p130^{-/-}$ and age-matched WT animals were histologically analyzed at P30. Semithin toluidine blue WT and $p130^{-/-}$ cochlear cross sections revealed clear evidence of supernumerary epithelial cells, particularly in the apical and middle turns of $p130^{-/-}$ cochleae (Fig. 3*A–F*). Whole-mount preparations of $p130^{-/-}$ and WT cochleae immunolabeled with antibodies against myosin VIIa (Myo7a), Sox2, and β-tubulin, known markers for HCs, SCs, and nerve fibers, respectively, revealed the identity and organization of the supernumerary cells and their associated neural processes along the longitudinal axis of $p130^{-/-}$ mice cochleae (Fig. 4*A–U*). Compared with the OC phenotype of $Rb1^{-/-}$ mice, in which both supernumerary HCs and SCs were found in markedly high numbers (Mantela et al., 2005; Sage et al., 2005, 2006), $p130^{-/-}$ OC was similarly, but less profoundly, affected (Fig. 3*A–F*). No gender differences in OC phenotype were observed for the $p130^{-/-}$ animals analyzed in this study.

Impact of p130 deletion on HCs

Additional rows of OHCs were commonly found extending along the length of the apical and upper middle turns in $p130^{-/-}$ co-

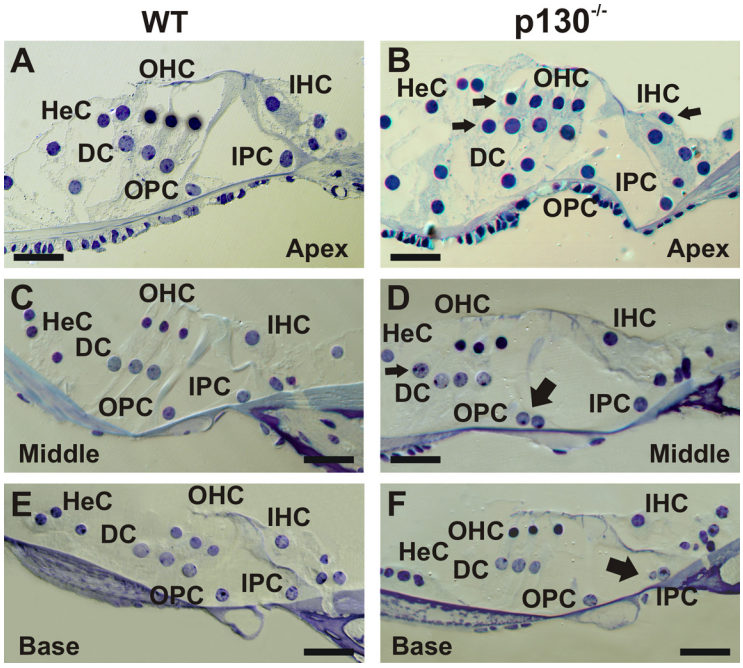

Figure 3. Morphological analysis of P30 p130 $^{-/-}$ and WT mouse OC. ***A–F***, Semithin (3 μm) plastic sections of apical, middle, and basal turns of the OC stained with toluidine blue show additional inner and outer hair cells (thin arrows) mostly concentrated in the apical region of the cochlea. Supernumerary pillar cells and particularly Deiters' cells (thick arrows) are found in different regions of the length of the cochlea, but more often observed in the apical and middle turns of p130 $^{-/-}$ cochlea. IHC, Inner hair cells; IPC, inner pillar cells; OPC, outer pillar cells; OHC, outer hair cells; DC, Deiters' cells; HeC, Hensen's cells. Scale bar, 10 μm.

chleae (Figs. 3*B*, 4*A*,*D*). On average, four rows of OHCs were observed in p130 $^{-/-}$ apex (Figs. 3*B*, 4*A*,*D*). Occasionally, a fifth OHC row was observed in a small fraction of p130 $^{-/-}$ mice analyzed histologically (data not shown). Similarly, two (87% of individuals) or three rows of IHCs (13%) were observed exclusively in p130 $^{-/-}$ mice in the apical turn positioned adjacent to the normal row of IHCs and curved along the spiral in the ordinary manner (Figs. 3*B*, 4*A*,*D*). Overall, p130 $^{-/-}$ mice had significantly more OHCs and IHCs in the apical and upper middle turns ($p < 0.01$) than their counterparts. Of note, 22% of the p130 $^{-/-}$ mice analyzed in this study also exhibited scattered supernumerary OHCs and IHCs in the middle and base of the OC, whereas none were detected in WT control animals. However, unlike the apical regions of the cochlea, these additional cells were arranged either as single extra cells or as short stretches typically consisting of 2–10 cells (Fig. 4*J*,*P*). Overall, lower middle and basal turns of p130 $^{-/-}$ cochleae showed a rather normal hair cell distribution (i.e., 3:1 OHC to IHC ratio) when compared with the apical regions.

Like ordinary HCs in WT animals, supernumerary rows of OHCs and IHCs in p130 $^{-/-}$ OC were labeled with the HC marker Myo7a (Fig. 4*A*,*D*). Moreover, ectopic Myo7a-positive cells were occasionally detected outside the OC, yet their presence was limited to the apical portion of the cochlea (Fig. 4*A*, arrow). Also notable was the observation that extra OHC rows appear capable of attracting peripheral processes of nerve fibers, as indicated by the presence of β-tubulin immunostaining of neural processes running alongside each row of OHCs throughout the length of the cochlea. Note the presence of four rows of spiraling nerve fibers in the cochlear apex and middle turn shown in Figure 4, *F* and *L*, in contrast to the typical three rows observed in WT animals (Fig. 4*I*,*O*).

Impact of p130 deletion on SCs

Consistent with p130 protein expression in SCs throughout OC postnatal development (Fig. 1), deficiency of the p130 gene directly affects SC density (Fig. 3*B*,*D*,*F*). As suggested by cross-sectional analyses, additional rows of Sox2-positive cells were observed in whole-mount apical and upper middle turns of p130 $^{-/-}$ OC; however, they appeared to be less organized than those in WT littermate cochleae (Fig. 4*B*,*E*,*H*,*K*,*N*). The number of Deiters' cell rows in the apical turn of the p130 $^{-/-}$ mice was significantly higher ($p < 0.01$) than that observed in the upper middle turn. Contrasting with the three rows of Deiters' cells commonly observed throughout the length of the WT OC, two (57%) or three (43%) additional rows of Deiters' cells were present in the apical turn of p130 $^{-/-}$ OC. Conversely, one (65.2%), two (26.1%), or three (8.7%) supernumerary rows of Deiters' cells were counted in the upper middle turn of the OC of the p130 $^{-/-}$ mice (Fig. 4*B*,*E*,*K*). Moreover, additional individual Deiters' cells, but not rows, were observed in the lower middle and basal turns of p130 $^{-/-}$ cochlea (Fig. 4*Q*). As a whole, cross-sectional and whole-mount analyses revealed an increase in the number of Deiters' cell bodies relative to OHCs; although a 1:1 OHC to Deiters' cell ratio was observed throughout the entire length of WT mice OC, p130 $^{-/-}$ mice exhibited at least one extra unpaired row of Deiters' cells (Fig. 3*D*,*E*). Similar results have been previously described in the OC of *Cdkn1b*-null mice (Löwenheim et al., 1999).

The presence of extra pillar cells in p130 $^{-/-}$ OC was initially suggested by cross-sectional and whole-mount preparations (Figs. 3*D*,*F*, 4*K*) and confirmed by p75 ^{NTR} and α-tubulin immunolabeling (Fig. 5*A–D*). However, when compared with additional Deiters' cells, supernumerary pillar cells were not organized into additional rows. Instead, they were sparsely distributed throughout the different regions of the cochlea, but particularly concentrated in the upper middle turn of the cochlea (Fig. 5*D*). Interestingly, Hensen's cells, which normally show affinity to p75 ^{NTR} antibody, were not labeled with this antibody in p130 $^{-/-}$ OC (Fig. 5*B*).

All things considered, our current analyses suggest a near-normal lower middle and basal turn OC in p130 $^{-/-}$ despite a few extra OHCs and IHCs, peripheral nerve fibers, as well as a few extra Deiters' and pillar cells distributed throughout the length of the lower middle and basal turns of the p130 $^{-/-}$ cochleae. Whether the additional fibers are afferent in nature and a direct result of increased projections or redistribution of existing afferent fibers remains to be determined.

Cell proliferation in p130 $^{-/-}$ OC

To test whether supernumerary cells were generated through cell cycle dysregulation, P21 and P30 p130 $^{-/-}$ and WT mice were injected with the thymidine analog EdU (50 mg/kg) and killed 4 h after injection. A total of 12 mice (3 per age group for each genotype) were analyzed for EdU incorporation. No labeling was observed at either P21 (Fig. 6*A*,*B*) or P30 (data not shown) WT

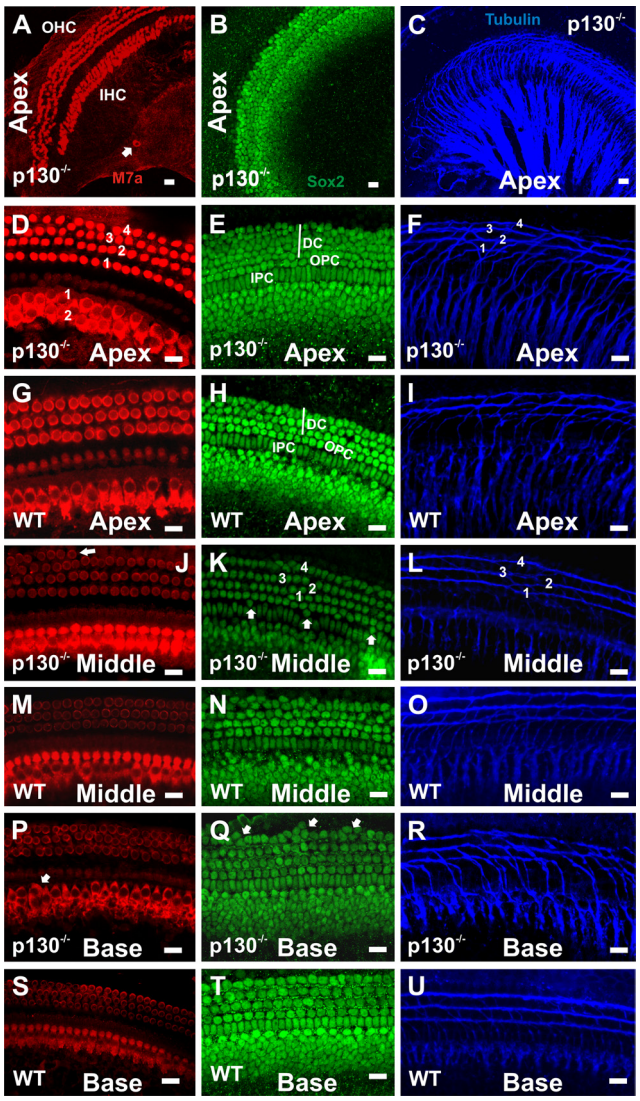

Figure 4. Immunohistochemical detection of myosin VIIa (Myo7a), Sox2, and β-tubulin expression in P30 p130 $^{-/-}$ and WT cochlea. ***A–I***, Comparable with the WT control animals, additional rows of sensory HCs and SCs were readily observed, staining uniformly with Myo7a (red) and Sox2 (green), respectively. Moreover, tubulin (blue) staining suggests that additional rows of sensory cells attracted nerve fibers based on the presence of supernumerary peripheral neural processes tracking adjacent to additional rows of cells. The presence of associated neural processes onto ectopic HCs was also seen in the apical turn of the p130 $^{-/-}$ cochlea. ***J–U***, Additional HCs and SCs were also observed in the lower middle and basal turns of p130 $^{-/-}$ cochleae; however, in contrast to the apical and upper middle turns, they do not form long rows of cells but rather are observed intermittently. Similar to the apex and middle turns, additional peripheral neural processes were observed and correspond to areas where supernumerary HCs were observed. The arrow in ***A*** indicates ectopic Myo7a-positive cell in the apical turn of p130 $^{-/-}$ cochlea. Additional arrows throughout the panel indicate supernumerary HCs and SCs; the numbers in ***D*** and ***K*** indicate rows of supernumerary cells, whereas the numbers in ***F*** and ***L*** correspond to spiraling tracts of peripheral neural fibers. IHC, Inner hair cells; IPC, inner pillar cells; OPC, outer pillar cells; OHC, outer hair cells; DC, Deiters' cells. Scale bar, 10 μm.

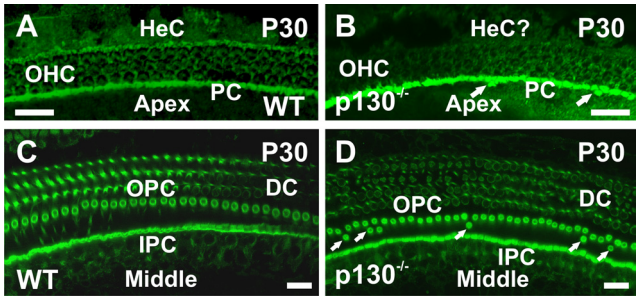

Figure 5. Immunohistochemical localization of p75 ^{NTR} and acetylated α-tubulin in adult (P30) mouse OC confirmed supernumerary pillar cells in p130 $^{-/-}$ OC. Contrasting with the WT control animals (***A***), additional p75 ^{NTR}-positive pillar cells (arrows) were observed in the apical (***B***) and middle turns (data not shown) in p130 $^{-/-}$ OC. Interestingly, although WT animals showed conspicuous p75 ^{NTR} immunoreactivity in Hensen's cells (***A***), no immunolabeling was observed in p130 $^{-/-}$. Moreover, acetylated α-tubulin, which labels pillar cells and Deiters' cell phalangeal processes, was used to verify p75 ^{NTR} data. Although no additional SCs were observed in the WT animals (***C***), additional pillar cells were located at the apical (data not shown) and middle turn (***D***, arrows) of p130 $^{-/-}$ cochleae. HeC, Hensen's cells; OPC, outer pillar cells; IPC, inner pillar cells; OHC, outer hair cells; DC, Deiters' cells. Scale bar, 10 μm.

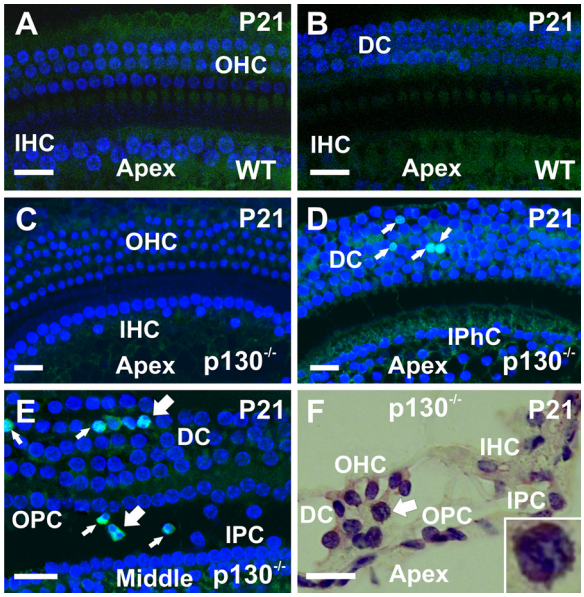

Figure 6. Unscheduled SC proliferation in adult p130 $^{-/-}$ mouse OC. ***A–E***, Whole-mount preparations of the OC of P21 and P30 WT and p130 $^{-/-}$ mice were assessed for unscheduled cell cycle reentry using EdU. All tissues were counterstained with DAPI. No labeling was observed at either time point in WT cochleae at either the HC (***A***) or SC (***B***) level. Likewise, no signs of proliferation were observed in P30 p130 $^{-/-}$ OC (data not shown). ***C***, EdU staining was not observed in p130 $^{-/-}$ HCs; however, positive Deiters' and pillar cells were detected in the apical and upper middle turns of the p130 $^{-/-}$ mice OC. ***D***, Most cells that incorporated EdU in the apical turn were found to be in S-phase; however, cells apparently in telophase (***E***, thick arrows) were also observed. ***F***, Unscheduled proliferation in the p130 $^{-/-}$ OC was also detected in cross-sectional analyses of the apical turn showing Deiters' cells apparently in the late stage of prophase. Very condensed chromosomes were seen in several Deiters' cells of this specific individual, and particularly visible in the nucleus indicated by the arrow and shown in detail. The thin arrows in ***D*** and ***E*** indicate cell in S-phase. The thick arrows in ***E*** and ***F*** point to cells at different stages of mitotic division. OHC, Outer hair cells; IHC, inner hair cells; DC, Deiters' cells; OPC, outer pillar cells; IPC, inner pillar cells; IPhC, inner phalangeal cells. Scale bar, 10 μm.

cochleae; likewise P30 p130 $^{-/-}$ mouse cochleae exhibited no signs of proliferation (data not shown). Moreover, no EdU incorporation was detected in regular or supernumerary HCs at P21 in p130 $^{-/-}$ OC (Fig. 6*C*). However, several EdU-positive nuclei in the Deiters' and pillar cell regions were apparent in the apical and upper middle turns of the p130 $^{-/-}$ cochlea (Fig. 6*D*,*E*). On average, eight EdU-positive nuclei were observed per cochlea. Most of those nuclei appeared to be in S-phase (Fig. 6*D*,*E*, thin arrows). Moreover, few EdU-positive cells were identified in the upper middle turn and appeared to be at later stages of mitotic division, as assumed from the observation of small, adjacent pairs of labeled nuclei (Fig. 6*E*, thick arrows). Additional indication of unscheduled proliferation in p130 $^{-/-}$ OC came from cross-sectional analyses of the apical turn of P21 p130 $^{-/-}$ mice showing a few nuclei apparently in the late stage of prophase in the

region normally occupied by the Deiters' cells (Fig. 6*F*, thick arrow).

Mechanism of cell proliferation in p130 $^{-/-}$ OC

Several genes, including *Cdkn1b* and *Rb1*, regulate proliferation and differentiation in the developing auditory epithelium (Chen and Segil, 1999; Mantela et al., 2005; Sage et al., 2005, 2006; Minoda et al., 2007). As a bona fide inhibitor of the cell cycle, CDKN1B is present in several types of SCs in the mature OC (Kanzaki et al., 2006; Minoda et al., 2007; Ono et al., 2009). Similar to p130 $^{-/-}$, silencing the *Cdkn1b* gene in mature OC has been shown to stimulate SC proliferation (Kanzaki et al., 2006; White et al., 2006; Minoda et al., 2007). Moreover, in the mature OC, *Rb1* appears to be one of the primary growth inhibitors, keeping HCs and to some extent SCs in their quiescent state (Mantela et al., 2005; Sage et al., 2005, 2006). Together, *Cdkn1b* and the pRB family are crucial components of the cell cycle checkpoint in the inner ear and beyond. To investigate the molecular mechanism responsible for unscheduled proliferation and generation of supernumerary SCs in adult p130 $^{-/-}$ mouse OC, we examined the expression of *Cdkn1b*, *Rb1*, and p107 in P30 WT and p130 $^{-/-}$ mouse OC. Expression of CDKN1B in adult WT mice cochleae was confirmed (Fig. 7*A*). However, both CDKN1B protein and relative transcript expression were found to be downregulated in the p130 $^{-/-}$ OC (Fig. 7*C*,*E*). Interestingly, changes in both *Rb1* and p107 relative abundances were not significantly different in p130 $^{-/-}$ OC (Fig. 7*E*). Of note, residual p130 mRNA was detected in the knock-out mouse OC (Fig. 7*E*). To validate functional knock-out of the p130 gene in the mouse inner ear, P30 WT and p130 $^{-/-}$ cochleae were dissected and submitted to Western blot analysis using the p130 antibody previously used in the immunolabeling study. In addition, liver biopsies in which p130 is known to be expressed (Calvisi et al., 2009) were collected from WT and p130 $^{-/-}$ animals and used as control tissues. This antibody targets amino acids 416–516 of the p130 protein, well beyond the frameshift mutation carried by the p130 $^{-/-}$ mouse. A band of ~128 kDa, which corresponds to the predicted molecular weight of p130, was identified in both liver and cochlear extracts of the WT animals but was completely absent in p130 $^{-/-}$ mice (Fig. 7*F*). Therefore, no functional protein was detected in the knock-out mouse by either immunostaining (data not shown) or Western blot analyses (Fig. 7*F*). Furthermore, we confirmed the truncating mutation as previously described (Cobrinik et al., 1996) by sequencing and comparison analyses of the WT and p130 knock-out gene PCR product. The p130 knock-out construct removed a portion of exon 2, leaving exons 1 and 3–22 intact, including the 3′-UTR, the latter being targeted by the TaqMan assay used in this study. Residual p130 mRNA in p130 $^{-/-}$ mice may be the result of alternative splicing around the knock-out allele, even though no protein was apparent by Western blot using antibodies directed at epitopes encoded by either exons 9–12 (Fig. 7*E*) or the last 50 aa encoded by exon 22 (Cobrinik et al., 1996).

Physiological phenotype in the absence of a functional p130 gene

To understand the functional impact of extra cells in the OC of p130 $^{-/-}$ mice, ABRs were recorded to evaluate the functional integrity of the auditory pathway of a group of nine P30 p130 $^{-/-}$ mice. The histological phenotype described previously was verified in the animals characterized physiologically. Although slight variations in the morphology of the waveform were observed from individual to individual, its overall form resembled ABRs from mammals in general, consisting of four or five positive-going voltage peaks that occur within 10 ms of stimulation (Fig. 8*A*,*B*). Average thresholds to tone pip stimuli spanning the frequency range over which normal mice are sensitive to airborne sound were not significantly different from those of control animals ($F_{(1,19)} = 0.058$). However, <12 kHz, thresholds of p130 $^{-/-}$ mice were consistently elevated, although the amount of elevation was always ≤10 dB (Fig. 8*C*).

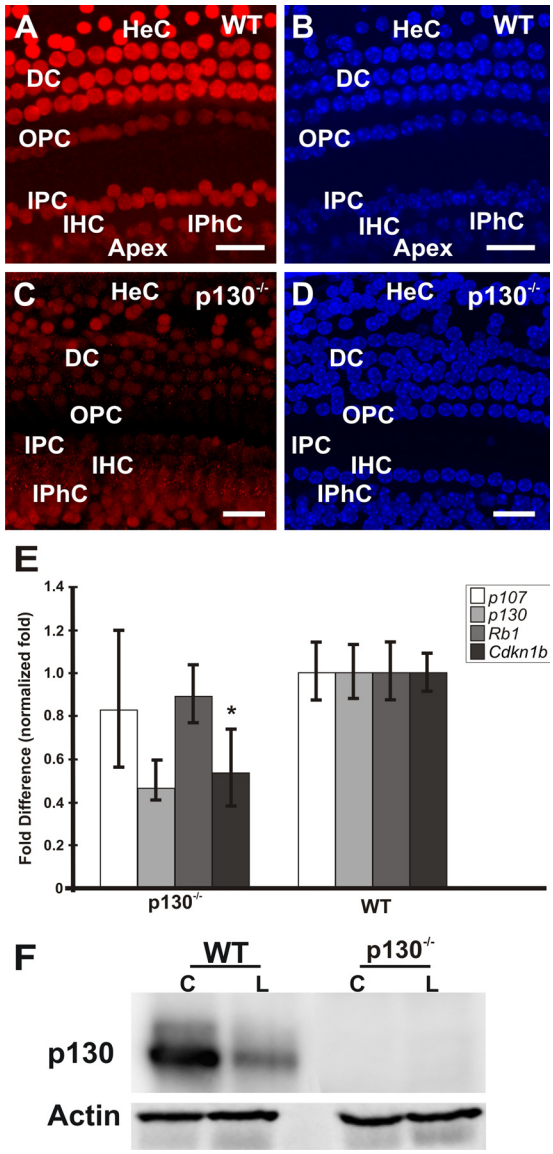

Figure 7. p130 deficiency effect on other negative cell cycle regulators. ***A***, CDKN1B immunolabeling in the apical turn of P30 WT whole-mount mouse OC counterstained with DAPI (***B***) revealed a radial gradient of expression in SCs with Hensen's cells showing higher levels of expression, followed by the Deiters' and pillar cells. CDKN1B expression was also detected in cells from the greater epithelial ridge (GER) area. ***C***, In contrast, immunolabeling of the apical turn of p130 $^{-/-}$ mouse OC on P30 counterstained with DAPI (***D***) suggested CDKN1B overall downregulation, particularly in Deiters' cells. ***E***, Corroborative evidence reveals that relative abundance of *Cdkn1b* mRNA expression in the p130 $^{-/-}$ mice OC on P30 was significantly downregulated ($p < 0.01$) when compared with the WT animals. No statistical differences in *Rb1* and p107 mRNA relative abundance were observed between WT and p130 $^{-/-}$ cochleae. ***F***, Immunoblot analysis of p130 levels in cochleae of WT and p130 $^{-/-}$ animals on P30 confirms p130 $^{-/-}$ functional knock-out. Liver lysates (L) prepared from WT and p130 $^{-/-}$ mice were used as positive and negative controls, respectively. β-Actin was used as loading control. IHC, Inner hair cells; IPC, inner pillar cells; OPC, outer pillar cells; DC, Deiters' cells; HeC, Hensen's cells; IPhC, inner phalangeal cells. C, Cochleae; L, liver. Scale bar, 20 μm. *$p < 0.01$.

DPOAEs were used to assess the status of mechanoelectrical transduction in p130$^{-/-}$ mice compared with WT animals. Based on levels of the $2f_1$–f_2 distortion product measured in the external ear canal, DPOAEs from knock-out mice were not statistically different from those of control animals. However, there was a trend for emissions recorded at f_2 frequencies between 5 and 14 kHz for the 60 dB SPL condition (Fig. 9*A*), and between 5.8 and 12 kHz for the 40 dB SPL condition (Fig. 9*B*), to be consistently reduced in knock-out animals relative to those observed in normal controls. The largest DPOAE level difference between control and mutant animals was 14 dB at 6.7 kHz and 13 dB at 8.7 kHz for the 60 and 40 dB primary levels, respectively, with low- and high-frequency roll-offs of ~29 and 13 dB/octave (Fig. 9*C*). Differences between genotypes spanned a stimulus frequency bandwidth of 1 and 1.4 octaves for the 40 and 60 dB SPL primary level conditions, respectively.

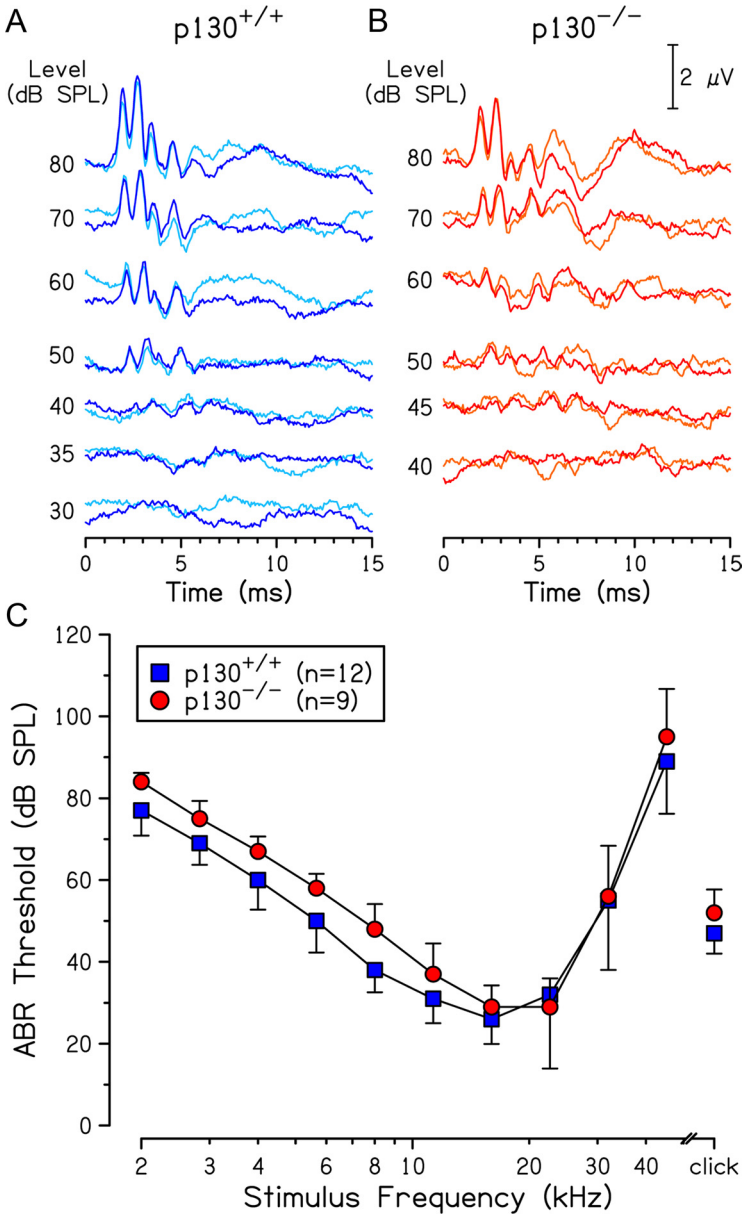

Figure 8. Auditory brainstem responses in p130$^{-/-}$ mice. ***A***, ***B***, Representative examples of replicated ABR waveforms for a wild-type (***A***) and p130$^{-/-}$ mouse (***B***) in response to several levels of an 8 kHz tone burst. ***C***, Average ABR thresholds are shown as a function of stimulus frequency for WT and p130$^{-/-}$ mice. Error bars, shown in one direction for clarity, represent 1 SD.

Discussion

Using a variety of approaches, we have shown that the p130 gene is developmentally regulated and influences cell quiescence within the mouse OC. Initially detected in SCs at P0 throughout the length of the cochlea, HCs and SCs p130-positive nuclei follow an apex-to-base gradient from P14 onward. Likewise, real-time quantitative PCR revealed that p130 mRNA levels are the lowest during periods of mitotic activity (E12.5–E13.5) but are progressively increased in the postmitotic OC. Reflecting the cell growth suppression role of p130 (Mulligan and Jacks, 1998; Choi et al., 2002; Burkhart and Sage, 2008), p130$^{-/-}$ mice produce supernumerary HCs and SCs, with SCs still proliferating in the young adult p130$^{-/-}$ OC (Fig. 6). Together, these data support the regulatory role of p130 influencing cell cycle arrest and quiescence of postmitotic SCs and, to a less extent, HCs in the mouse OC. Complementary to these findings, *Rb1* is highly expressed in the base of the cochlea and follows a base-to-apex gradient in adults (Mantela et al., 2005). The ability of pRBs to compensate for one another is well established (Cobrinik et al., 1996; Mulligan and Jacks, 1998). In the cochlea, *Rb1* appears to play a more important role in the maintenance of cell quiescence than does p130, and appears to compensate for p130 expression deficiencies in the base and at least partially in the remaining two-thirds of the cochlea. Furthermore, although we have no evidence at this time that supernumerary SCs undergo transdifferentiation, our working hypothesis is that additional HCs observed in the p130$^{-/-}$ OC are the product of SC trandifferentiation earlier in development. A phenomenon observed *in vitro* through down-regulation of the cell cycle inhibitor *CdKn1b* (White et al., 2006). In this regard, conditional *Rb1* deletion in Deiters' and pillar cells supports our premise that pocket protein manipulation in quiescent SCs is sufficient to bring them back into the cell cycle (Yu et al., 2010). Nevertheless, newly generated SCs through *Rb1* deletion have a transient life, dying shortly after generation (Mantela et al., 2005; Sage et al., 2006; Yu et al., 2010), a finding that stands in stark contrast to our observation that HCs and SCs in p130$^{-/-}$ mice appear to survive.

Maintenance of postmitotic growth arrest is controlled by a network of interacting molecules that regulate activity of the E2F family of transcription factors. All three pRBs have well established roles as direct repressors of E2F activity that, in turn, promotes cell growth arrest (Cobrinik, 2005). *Rb1* has been implicated as the major regulator of postmitotic quiescence and survival in HCs (Mantela et al., 2005; Sage et al., 2005, 2006), whereas our evidence suggests that p130 also affects SC quiescence in the mouse OC (Figs. 3–5). Together, previously pub-

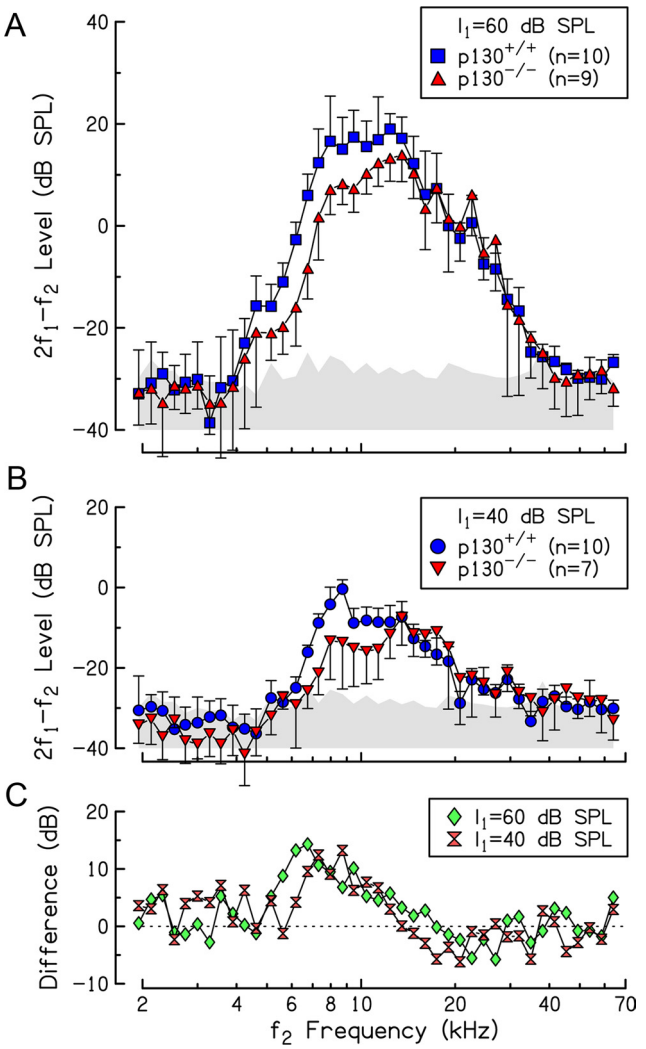

Figure 9. DPOAEs in $p130^{-/-}$ mice. ***A***, ***B***, Average DPOAE levels are shown as a function of f_2 frequency for WT and $p130^{-/-}$ mice in response to f_1 levels (l_1) of 60 dB SPL (***A***) and 40 dB SPL (***B***). Average noise floor plus 1 SD is shown as the upper boundary of the shaded area in ***A*** and ***B***. ***C***, Differences in the level of DPOAEs between WT and $p130^{-/-}$ mice are shown as a function of f_2 frequency at the primary levels shown in ***A*** and ***B***. Error bars, shown in one direction only for clarity, represent 1 SD.

lished studies and our current results suggest that, despite their similar origin, HC and SC postmitotic quiescence may be achieved and maintained through different mechanisms, with *Rb1* and p130 playing roles in HC and SC quiescence machinery, respectively.

Alongside *Rb1*, the CKI *Cdkn2d* ($p19^{ink4d}$) has been shown to regulate cell cycle checkpoint and mitotic quiescence of HCs, whereas *Cdkn1b* appears to play a similar role in the regulation of SC proliferation (Mantela et al., 2005; Sage et al., 2005, 2006; Laine et al., 2007). Indeed, *in vitro* studies have shown that isolated SCs from the postnatal mouse cochlea downregulate *Cdkn1b* before proliferating/transdifferentiating into HCs (White et al., 2006). Like p130, *Cdkn1b* upregulation promotes cellular differentiation and quiescence, whereas its downregulation is correlated with mitogenic stimulation (Philipp-Staheli et al., 2001). Moreover, it has been suggested that *Hes1*-mediated proliferation of precursor cells in the OC, thymus, and liver is achieved through *Cdkn1b* transcriptional repression (Murata et al., 2009). Although the precise mechanism underlying p130-mediated maintenance of SC quiescence in the mouse OC is unknown, the coincident expression pattern of p130 and CDKN1B in the mouse cochlea (Chen and Segil, 1999; Kanzaki et al., 2006; Murata et al., 2009; Ono et al., 2009), certain similarities in the postnatal OC morphology shared by $p130^{-/-}$ and *Cdkn1b* knockdown mice (Kanzaki et al., 2006; Ono et al., 2009), as well as our present results showing *Cdkn1b* mRNA and protein downregulation in $p130^{-/-}$ OC, have led us to postulate that p130 mediates SC quiescence through *Cdkn1b*.

The ability of the pRBs to exert their growth-suppressive activity is dependent on their interaction with transcription factors, such as the family of E2F/DP molecules (Dyson, 1998). The p130 protein is the predominant pRB family member bound to E2F-regulated promoters in quiescent cells and is known to form an evolutionarily conserved multisubunit protein complex with E2F4. Moreover, the p130/E2F4 complex is necessary for pocket protein-mediated cell cycle arrest and repression of cell cycle-dependent genes (Litovchick et al., 2007). In contrast to the common picture of pocket protein inactivation through phosphorylation by cyclin-dependent kinases (CDKs), p130/E2F4-mediated mitotic arrest is thought to be arbitrated through p130 phosphorylation by glycogen synthase kinase 3 (Mayol et al., 1996; Litovchick et al., 2004). Moreover, additional posttranslational deacetylation of p130 by histone deacetylases after cell cycle exit changes its interaction with other non-cell cycle-related proteins (Jackson et al., 2005; Popov et al., 2005), a finding consistent with the role of p130 in cell cycle exit and mitotic quiescence. Ultimately, p130 downregulation is directly proportional to E2F4 upregulation, resulting in unscheduled, low-rate cell proliferation in otherwise quiescent cells (Poplawski and Nauman, 2008).

$p130^{-/-}$ mouse retains near-normal peripheral auditory sensitivity despite the presence of supernumerary cells

The nearly normal sensitivity of $p130^{-/-}$ mice to sound stimulation was an unanticipated finding given the presence of supernumerary HCs and SCs and the gross functional abnormalities observed in other cell cycle-related gene knock-out mouse models (Chen and Segil, 1999). Although a small number of mammalian species normally exhibit more than three rows of OHCs in the cochlear apex (for review, see Echteler et al., 1994), additional HC rows have not been described in mice and the natural expectation was that changes in the mass and possibly the stiffness of the OC in $p130^{-/-}$ mice, as well as altered interactions among transduction elements operating at the micromechanical level, would lead to an abnormal physiological phenotype. Although the physiology finding was unexpected, it is interesting and clearly draws attention to the many aspects of peripheral auditory physiology that remain unexplored in the $p130^{-/-}$ mouse, including more detailed analyses of mechanoelectrical transduction. Regardless of the outcome of the effort to better understand transduction biomechanics and neural processing in the $p130^{-/-}$ mouse, the fact remains that auditory sensitivity in mice with p130 deletions appears normal, and that finding reinvigorates the discussion of mammalian HC regeneration via the agency of cell cycle manipulation. Although supernumerary HCs and SCs are evident in the $p130^{-/-}$ mouse OC, the increase in the size of both cell populations is moderate. When combined with the observations that the fundamental cytoarchitecture of the end organ is maintained and sensitivity to sound is essentially normal in P30 animals, one is left to consider the possibility that p130 deficiency leads serendipitously to a balance of progenitor cell

proliferation and differentiation within an otherwise postmitotic inner ear, without significantly affecting OC homeostasis.

p130 gene as a potential therapeutic target for SC-mediated HC regeneration

As a whole, this study adds to a more informed understanding of the functional role played by the pocket proteins in the inner ear. The histological and physiological cochlear phenotype in $p130^{-/-}$ mice suggests a role for p130-mediated SC quiescence in the apical and upper middle turns of the cochlea. Although therapeutic reinitiation of the cell cycle in the postmitotic mammalian inner ear is a work in progress, results of the present study add to the proof of principle of HC regeneration through cell cycle manipulation. Although mediators of p130 function in the OC have yet to be identified, a possible mechanism underlying p130-mediated supernumerary HC and SC generation would likely involve a variety of players, including *Rb1*, *Cdkn1b*, and *E2f4*, a conclusion that illuminates the intricacy of the process. Nevertheless, although direct manipulation of *Rb1* or *Cdkn1b* produces less than optimal outcomes (i.e., loss of architectural homeostasis and loss of physiologic function) (Chen and Segil, 1999; Chen et al., 2003; Mantela et al., 2005; Sage et al., 2006; Yu et al., 2010), p130 manipulation may offer an alternative intervention path, in which the expression of major cell cycle controllers can be manipulated through p130 conditional elimination. Notably, despite its role in cell cycle progression and cellular growth arrest, mutations in the p130 gene alone have not been associated with any type of human malignancy (Burkhart and Sage, 2008; Worley et al., 2010), arguing in favor of its intrinsic value as a therapeutic tool to manipulate SC cell proliferation and, perhaps, HC regeneration. A better understanding of HC and SC cell cycle regulation and the mechanism(s) underlying p130 in cell quiescence and proliferation in the OC, combined with targeted and controlled inhibition of p130 function in the adult OC, are likely to enhance our ability to manipulate SC proliferation, bringing us closer to the ultimate goal of regenerating HCs in the deafened cochlea.

References

Burkhart DL, Sage J (2008) Cellular mechanisms of tumor suppression by the retinoblastoma gene. Nat Rev Cancer 8:671–682.

Cafaro J, Lee GS, Stone JS (2007) Atoh1 expression defines activated progenitors and differentiating hair cells during avian hair cell regeneration. Dev Dyn 236:156–170.

Calvisi DF, Ladu S, Pinna F, Frau M, Tomasi ML, Sini M, Simile MM, Bonelli P, Muroni MR, Seddaiu MA, Lim DS, Feo F, Pascale RM (2009) SKP2 and CKS1 promote degradation of cell cycle regulators and are associated with hepatocellular carcinoma prognosis. Gastroenterology 137:1816–1826.e1–10.

Chen P, Segil N (1999) p27(Kip1) links cell proliferation to morphogenesis in the developing organ of Corti. Development 126:1581–1590.

Chen P, Zindy F, Abdala C, Liu F, Li X, Roussel MF, Segil N (2003) Progressive hearing loss in mice lacking the cyclin-dependent kinase inhibitor Ink4d. Nat Cell Biol 5:422–426.

Choi HH, Jong HS, Hyun Song S, You Kim T, Kyeong Kim N, Bang YJ (2002) p130 mediates TGF-beta-induced cell-cycle arrest in *Rb1* mutant HT-3 cells. Gynecol Oncol 86:184–189.

Cobrinik D (2005) Pocket proteins and cell cycle control. Oncogene 24:2796–2809.

Cobrinik D, Lee MH, Hannon G, Mulligan G, Bronson RT, Dyson N, Harlow E, Beach D, Weinberg RA, Jacks T (1996) Shared role of the pRB-related p130 and p107 proteins in limb development. Genes Dev 10:1633–1644.

Cotanche DA (1997) Hair cell regeneration in the avian cochlea. Ann Otol Rhinol Laryngol Suppl 168:9–15.

Duncan LJ, Mangiardi DA, Matsui JI, Anderson JK, McLaughlin-Williamson K, Cotanche DA (2006) Differential expression of unconventional myosins in apoptotic and regenerating chick hair cells confirms two regeneration mechanisms. J Comp Neurol 499:691–701.

Dyson N (1998) The regulation of E2F by pRB-family proteins. Genes Dev 12:2245–2262.

Echteler SM, Fay RR, Popper AN (1994) Structure of the mammalian cochlea. In: Comparative hearing: mammals (Fay RR, ed), pp 134–171. New York: Springer.

Hernández PP, Olivari FA, Sarrazin AF, Sandoval PC, Allende ML (2007) Regeneration in zebrafish lateral line neuromasts: expression of the neural progenitor cell marker sox2 and proliferation-dependent and-independent mechanisms of hair cell renewal. Dev Neurobiol 67:637–654.

Jackson MW, Agarwal MK, Yang J, Bruss P, Uchiumi T, Agarwal ML, Stark GR, Taylor WR (2005) p130/p107/p105Rb-dependent transcriptional repression during DNA-damage-induced cell-cycle exit at G_2. J Cell Sci 118:1821–1832.

Jones JE, Corwin JT (1993) Replacement of lateral line sensory organs during tail regeneration in salamanders: identification of progenitor cells and analysis of leukocyte activity. J Neurosci 13:1022–1034.

Kaiser CL, Kamien AJ, Shah PA, Chapman BJ, Cotanche DA (2009) 5-Ethynyl-2′-deoxyuridine labeling detects proliferating cells in the regenerating avian cochlea. Laryngoscope 119:1770–1775.

Kanzaki S, Beyer LA, Swiderski DL, Izumikawa M, Stöver T, Kawamoto K, Raphael Y (2006) p27(Kip1) deficiency causes organ of Corti pathology and hearing loss. Hear Res 214:28–36.

Kawamoto K, Ishimoto S, Minoda R, Brough DE, Raphael Y (2003) *Math1* gene transfer generates new cochlear hair cells in mature guinea pigs *in vivo*. J Neurosci 23:4395–4400.

Laine H, Doetzlhofer A, Mantela J, Ylikoski J, Laiho M, Roussel MF, Segil N, Pirvola U (2007) $p19^{Ink4d}$ and $p21^{Cip1}$ collaborate to maintain the postmitotic state of auditory hair cells, their codeletion leading to DNA damage and p53-mediated apoptosis. J Neurosci 27:1434–1444.

Litovchick L, Chestukhin A, DeCaprio JA (2004) Glycogen synthase kinase 3 phosphorylates RBL2/p130 during quiescence. Mol Cell Biol 24:8970–8980.

Litovchick L, Sadasivam S, Florens L, Zhu X, Swanson SK, Velmurugan S, Chen R, Washburn MP, Liu XS, DeCaprio JA (2007) Evolutionarily conserved multisubunit RBL2/p130 and E2F4 protein complex represses human cell cycle-dependent genes in quiescence. Mol Cell 26:539–551.

Löwenheim H, Furness DN, Kil J, Zinn C, Gültig K, Fero ML, Frost D, Gummer AW, Roberts JM, Rubel EW, Hackney CM, Zenner HP (1999) Gene disruption of $p27^{Kip1}$ allows cell proliferation in the postnatal and adult organ of corti. Proc Natl Acad Sci U S A 96:4084–4088.

Mantela J, Jiang Z, Ylikoski J, Fritzsch B, Zacksenhaus E, Pirvola U (2005) The retinoblastoma gene pathway regulates the postmitotic state of hair cells of the mouse inner ear. Development 132:2377–2388.

Mayol X, Garriga J, Grana X (1996) G_1 Cyclin/CDK-independent phosphorylation and accumulation of p130 during the transition from G_1 to G_0 leads to its association with E2F4. Oncogene 13:237–246.

Minoda R, Izumikawa M, Kawamoto K, Zhang H, Raphael Y (2007) Manipulating cell cycle regulation in the mature cochlea. Hear Res 232:44–51.

Morest DK, Cotanche DA (2004) Regeneration of the inner ear as a model of neural plasticity. J Neurosci Res 78:455–460.

Mulligan G, Jacks T (1998) The retinoblastoma gene family: cousins with overlapping interests. Trends Genet 14:223–229.

Murata J, Ohtsuka T, Tokunaga A, Nishiike S, Inohara H, Okano H, Kageyama R (2009) Notch-Hes1 pathway contributes to the cochlear prosensory formation potentially through the transcriptional down-regulation of p27Kip1. J Neurosci Res 87:3521–3534.

Ono K, Nakagawa T, Kojima K, Matsumoto M, Kawauchi T, Hoshino M, Ito J (2009) Silencing p27 reverses post-mitotic state of supporting cells in neonatal mouse cochleae. Mol Cell Neurosci 42:391–398.

Philipp-Staheli J, Payne SR, Kemp CJ (2001) $p27^{Kip1}$: regulation and function of a haploinsufficient tumor suppressor and its misregulation in cancer. Exp Cell Res 264:148–168.

Poplawski P, Nauman A (2008) Thyroid hormone—triiodothyronine—has contrary effect on proliferation of human proximal tubules cell line (HK2) and renal cancer cell lines (Caki-2, Caki-1)—role of E2F4, E2F5 and p107, p130. Thyroid Res 1:5.

Popov B, Chang LS, Serikov V (2005) Cell-cycle-related transformation of the E2F4–p130 repressor complex. Biochem Biophys Res Commun 336:762–769.

Rocha-Sanchez SM, Beisel KW (2007) Pocket proteins and cell cycle regulation in inner ear development. Int J Dev Biol 51:585–595.

Rocha-Sanchez SM, Morris KA, Kachar B, Nichols D, Fritzsch B, Beisel KW (2007) Developmental expression of Kcnq4 in vestibular neurons and neurosensory epithelia. Brain Res 1139:117–125.

Ruben RJ (1967) Development of the inner ear of the mouse: a radioautographic study of terminal mitoses. Acta Otolaryngol Suppl 220:221–244.

Sage C, Huang M, Karimi K, Gutierrez G, Vollrath MA, Zhang DS, García-Añoveros J, Hinds PW, Corwin JT, Corey DP, Chen ZY (2005) Proliferation of functional hair cells *in vivo* in the absence of the retinoblastoma protein. Science 307:1114–1118.

Sage C, Huang M, Vollrath MA, Brown MC, Hinds PW, Corey DP, Vetter DE, Chen ZY (2006) Essential role of retinoblastoma protein in mammalian hair cell development and hearing. Proc Natl Acad Sci U S A 103: 7345–7350.

Shou J, Zheng JL, Gao WQ (2003) Robust generation of new hair cells in the mature mammalian inner ear by adenoviral expression of Hath1. Mol Cell Neurosci 23:169–179.

Stone JS, Cotanche DA (2007) Hair cell regeneration in the avian auditory epithelium. Int J Dev Biol 51:633–647.

Taylor RR, Forge A (2005) Hair cell regeneration in sensory epithelia from the inner ear of a urodele amphibian. J Comp Neurol 484:105–120.

Walsh EJ, McGee J (2001) Hypothyroidism in the Tshr mutant mouse. In: Handbook of mouse auditory research: from behavior to molecular biology (Willot J, ed), pp 537–555. Boca Raton, FL: CRC.

Walsh EJ, McGee J, Javel E (1986) Development of auditory-evoked potentials in the cat. I. Onset of response and development of sensitivity. J Acoust Soc Am 79:712–724.

Weber T, Corbett MK, Chow LM, Valentine MB, Baker SJ, Zuo J (2008) Rapid cell-cycle reentry and cell death after acute inactivation of the retinoblastoma gene product in postnatal cochlear hair cells. Proc Natl Acad Sci U S A 105:781–785.

White PM, Doetzlhofer A, Lee YS, Groves AK, Segil N (2006) Mammalian cochlear supporting cells can divide and trans-differentiate into hair cells. Nature 441:984–987.

Woods C, Montcouquiol M, Kelley MW (2004) Math1 regulates development of the sensory epithelium in the mammalian cochlea. Nat Neurosci 7:1310–1318.

Worley MJ Jr, Landen CN, Slomovitz BM, Malpica A, Palla SL, Ramirez PT (2010) Expression of the retinoblastoma-related gene *Rb2*/p130 in the pathogenesis of serous carcinoma of the ovary. Appl Immunohistochem Mol Morphol 18:509–511.

Yamasoba T, Kondo K (2006) Supporting cell proliferation after hair cell injury in mature guinea pig cochlea *in vivo*. Cell Tissue Res 325:23–31.

Yu Y, Weber T, Yamashita T, Liu Z, Valentine MB, Cox BC, Zuo J (2010) *In vivo* proliferation of postmitotic cochlear supporting cells by acute ablation of the retinoblastoma protein in neonatal mice. J Neurosci 30:5927–5936.